

Simulation of mixed-phase clouds with the ICON-LEM in the complex Arctic environment around Ny-Ålesund

Vera Schemann¹ and Kerstin Ebell¹

¹University of Cologne, Institute for Geophysics and Meteorology, Cologne, Germany

Correspondence: Vera Schemann (vera.schemann@uni-koeln.de)

Abstract.

Low-level mixed-phase clouds have a substantial impact on the redistribution of radiative energy in the Arctic and are a potential driving factor for Arctic Amplification. To better understand the complex processes around mixed-phase clouds, a combination of long-term measurements and high-resolution modeling - which is able to resolve the relevant processes - is essential. In this study, we show the general feasibility of the new high-resolution model ICON-LEM to capture the general structure, type and timing of mixed-phase clouds at the Arctic site Ny-Ålesund and its potential and limitations for further detailed research. As a basic evaluation the model is confronted with data streams of single instruments including microwave radiometer and cloud radar, but also with value added products like the Cloudnet classification. The analysis is based on a 11-day long time period with selected periods being studied in more detail focusing on the representation of particular cloud processes, such as mixed-phase microphysics. In addition, targeted statistical evaluations against observational data sets are performed to assess i) how well the vertical structure of the clouds is represented and ii) how much information is added by higher horizontal resolutions. The results clearly demonstrate the advantage of high resolutions: in particular, with the highest horizontal model resolution of 75 m, the variability of liquid water path can be well captured. By comparing neighboring grid cells for different subdomains we also show the potential of the model to provide information on the representativity of single sites (as Ny-Ålesund) for a larger domain.

Copyright statement. TEXT

1 Introduction

The Arctic is warming at a higher rate than the global mean: the increase in the near-surface air temperature in the Arctic is more than twice as large as the observed increase in global mean temperature (Serreze and Barry, 2011; Wendisch et al., 2017). In order to better understand this phenomenon called Arctic amplification, many efforts are currently being undertaken to pinpoint and quantify the related feedback mechanisms causing the enhanced climate change signal (e.g., Wendisch et al., 2017; Screen et al., 2018; Goosse et al., 2018). Low-level mixed-phase clouds are known to be one potential driver for Arctic Amplification and are very common in the Arctic (Shupe et al., 2008), but especially under Arctic conditions, many climate

models struggle to capture these clouds depending on their microphysics parameterization (Pithan et al., 2014) and to represent
25 the boundary layer structure due to low and strong inversions. To improve the relevant parameterizations in climate models,
a better process understanding and formulation is necessary and can be obtained by creating a synthesis of state-of-the-art
observations and high-resolution process modeling.

Concerning observations, enhanced measurement capabilities during specific campaigns can be of great value (e.g., Wendisch
et al., 2019; Tjernström et al., 2019; Shupe et al., 2006). In particular, the upcoming MOSAiC campaign ([www.mosaic-](http://www.mosaic-expedition.org)
30 [expedition.org](http://www.mosaic-expedition.org)) will provide for the first time continuous observations of the atmosphere, ice and ocean in the central Arctic
over a full year. While such campaigns provide a wealth of information from various instrumentation also for the inner Arctic,
they are always limited to a certain time period. However, in order to understand a changing climate, long-term measurements
are crucial. Such observations are available at the French-German Arctic research station AWIPEV at Ny-Ålesund, Svalbard
(78.925°N, 11.930°E). Ny-Ålesund is located at the south coast of the Kongsfjord and is surrounded by glaciers and mountains
35 which affect the local climate (Maturilli et al., 2013; Maturilli and Kayser, 2017). AWIPEV operates comprehensive and state-
of-the-art instruments in particular for thermodynamic, aerosol, trace gas and surface radiation observations where some of the
observations have been started more than 30 years ago enabling trend analyses (Maturilli et al., 2015; Maturilli and Kayser,
2017). In 2016, a frequency-modulated continuous wave 94-GHz Doppler cloud radar of the University of Cologne (Küchler
et al., 2017) was installed at AWIPEV providing highly temporally and vertically resolved cloud observations and enabling the
40 analysis of microphysical processes of Arctic clouds in more detail at this site (Nomokonova et al., 2019; Gierens et al., 2019).

The complex surrounding of Ny-Ålesund creates its own need for high-resolution simulations to be able to capture the
surface heterogeneities caused by the mixed surrounding of mountains, flat land, glacier and the fjord. These conditions are
not feasible for the conventional idealized way to run Large-Eddy-Simulations with periodic boundary conditions and ho-
mogeneous surfaces (e.g. Klein et al., 2009; Ovchinnikov et al., 2014; Loewe et al., 2017). For this reason, we have applied
45 the new Icosahedral Nonhydrostatic (ICON) Large-Eddy-Model (LEM) for the first time in the Arctic. So far the model has
been mainly applied over Germany (Heinze et al., 2017; Marke et al., 2018) showing a reasonable representation of clouds
and turbulence. Our main research question thus is, if the ICON-LEM can reproduce the general structure of the observed
mixed-phase clouds at Ny-Ålesund by taking into account the complex topography. Beyond the general classification, we also
investigate how suitable the default microphysics and especially the parameterizations of cloud condensation nuclei (CCN)
50 and the ice nuclei (IN) (Hande et al., 2016) are for the Arctic regime. To investigate these questions, we picked a 11-day long
time period, i.e. from June 14 to June 24, 2017, during the ALOUD/PASCAL campaigns (Wendisch et al., 2019), where in
addition to the ground-based observations also aircraft-based remote sensing and in-situ observations have been performed in
the surroundings of Ny-Ålesund which will be used for further analysis in future.

The advantage of a large-eddy-simulation is that we can simulate at temporal and spatial scales, which are comparable to
55 the observations. However, due to computational costs, we always have to find a balance between resolution and domain size.
A rather small and limited domain comes with the need of large-scale forcing to capture the general synoptic situation. For
this reason, forcing from numerical weather prediction models has to be applied to get information about the synoptic situation
and the large scales. As the large-scale models are struggling with the Arctic conditions and especially the inversion strength

(e.g. Pithan et al. (2014); Neggers et al. (2019)), forcing from two different weather prediction models (Integrated Forecasting System (IFS) of the European Centre for Medium-range Weather forecasts (ECMWF) and the operational global ICON model by the German Weather Service (DWD) (Zängl et al., 2015)) have been used. The transition from large-scale forcing to the high-resolution simulations is a well-known difficulty: an inconsistent forcing might introduce artifacts in the high-resolution simulations or need very long spin-up times. This problem is mitigated by the new model suite ICON enabling a consistent forcing throughout the whole model hierarchy. We can use the operational weather forecast simulations and force our large-eddy-model with a consistent atmospheric state and a model setup, where only the respective parameterizations are switched off or are replaced by a more suitable version (e.g. for turbulence). We will show how beneficial this feature of the ICON family is and also look into the effect of increasing the horizontal resolution.

In this study, we demonstrate the general applicability of ICON-LEM in the Arctic, in particular in a place with a complex topography, to evaluate and study clouds. After a description of the general model setup (sec. 2.1) and the observations used (sec. 2.2), we will tackle our main research questions: Can the ICON-LEM capture the general structure of mixed-phase clouds at Ny-Ålesund characterized by the Cloudnet classification (sec. 3)? Is the consistent forcing within one model family beneficial (sec. 4.1)? Are the default microphysical parameterizations and a horizontal resolution of 75 m suitable for Arctic conditions (sec. 5 and sec. 5.2)? And can we use high-resolution simulations to evaluate the representativity of point measurements at complex locations (sec. 5.3)?

75 2 Setup

2.1 Model simulations

The Large-Eddy-Model of the ICON modeling system was developed during the HD(CP)² (High definition cloud and precipitation for advancing climate predictions) project and successfully tested and evaluated over Germany (Dipankar et al., 2015; Heinze et al., 2017). In this study, we show the first application of this model in the Arctic facing the difficult terrain and surface conditions around Ny-Ålesund. The setup consists of 4 different domains with one-way nesting. The largest domain has a horizontal resolution of 600 m, a 3 s timestep, and a domain size of 110 km. The smallest domain has 75 m resolution on a 20 km domain (Fig. 1), with a 3/8 s timestep. Due to the triangular grid, resolution in this context means edge length, which actually gives a 2/3 higher resolution in using the traditional definition in which resolution is the root of the cell area. The vertical resolution is the same for all horizontal resolutions and is highest close to the surface. The average vertical resolution between 500 m and 1.5 km is approximately 68 m. For the 11-day period between 14 June and 24 June 2017, every day is simulated separately with a new initialization at 0 UTC. The simulations are performed with the 2-moment microphysics scheme from Seifert and Beheng (2006) including 6 prognostic hydrometeors (water vapor, cloud water, cloud ice, rain, snow, hail, graupel) and a Smagorinsky turbulence scheme (Dipankar et al., 2015). The CCN and IN are described following a parameterization based on Hande et al. (2016). Due to the relatively small domain, the large-scale forcing is very important to capture the general synoptic situation. The forcing is applied only at the boundaries so that the flow can evolve and develop freely in the inner part of the domains. Nevertheless, the simulations depend on the large-scale forcing and different forcing

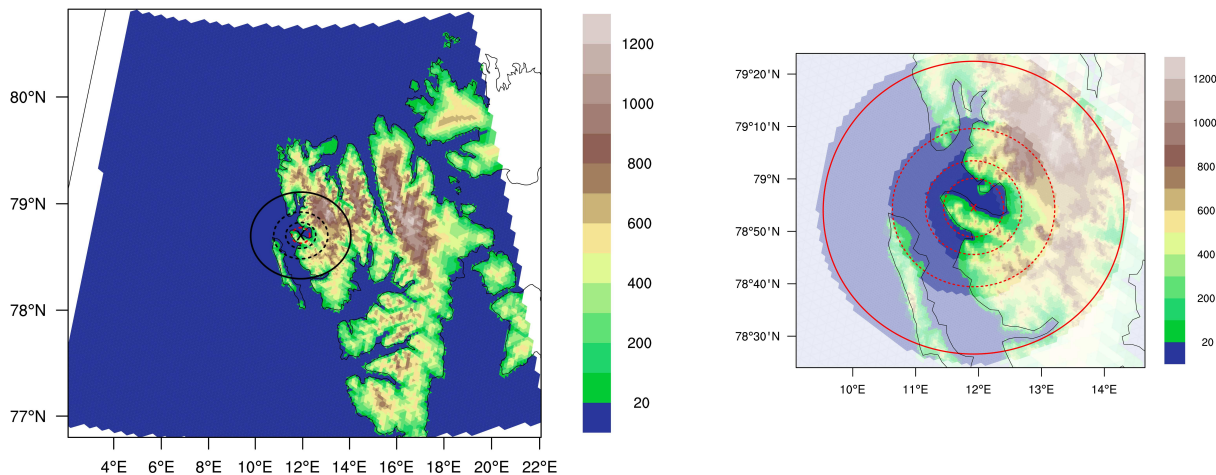


Figure 1. The topography (m), domain size and resolution around Ny-Ålesund for the 2 km ICON-NWP simulation (left) and the nested ICON-LEM simulations (right). The circles indicate the model domains for the 600 m, 300 m, 150 m, 75 m horizontal resolution model runs, respectively (from outer to inner circle) with corresponding domain sizes of approximately 110 km, 60 km, 35 km, and 25 km.

models can lead to different results. For this reason, we use two different models, i.e. the IFS in a horizontal resolution of $0.1^\circ \times 0.1^\circ$ and the operational global ICON forecasts in the R3B7 (approx. 13 km) resolution, and investigate the differences. A new forcing file is imported every hour for the IFS and every three hours for the ICON-global. While the IFS data profits from a rather high-resolution due to the fact that our study region is close to the pole, the ICON resolution stays constant due to the triangular grid structure at approx. 13 km, which is too coarse to force the ICON-LEM directly. For this reason, we introduced an intermediate step with approximately 2 km horizontal resolution and adjusted parameterizations (ICON-NWP) similar to the global simulations (see Fig. 1, left panel).

For the main part of the analysis, we use the so-called meteogram output, which is the column output at the grid-cell closest to the coordinates of the Ny-Ålesund measurements. The output is written every 9 seconds, which brings it close to the temporal resolution of the observational data sets. Due to the included topography and open boundaries, we expect the column to be representative for the conditions in Ny-Ålesund and by this provide a better estimate than traditional quantities like the domain mean or variance. Additionally, the weather is often large-scale driven and further affected by local topography and surface conditions which are accounted for in ICON-LEM. Nevertheless, these point-to-point comparisons can cause further uncertainties for model-observation comparisons, e.g. by missing clouds or certain structures which might be represented in neighbouring cells. For this reason, we also included the two-dimensional output of liquid water path (LWP) in our analysis, which has been written on 10-minute time intervals.

2.2 Observational data set

The model simulations are compared to observations performed at the atmospheric observatory of the Arctic French-German
110 research station AWIPEV at Ny-Ålesund. In this study, we use information from microwave radiometer and cloud radar obser-
vations and from a synergistic classification product.

The 94-GHz Doppler cloud radar of the University of Cologne (Küchler et al., 2017; Nomokonova et al., 2019) provides
vertical profiles of cloud radar reflectivity factor Z , Doppler velocity and spectral width up to a height of about 12 km. In
this study, we make use of the cloud radar reflectivity profiles which have been brought to a common 30-s and 20-m temporal
115 and height grid, respectively. In addition to the active component, the cloud radar also has a passive channel at 89 GHz. The
measured brightness temperatures at 89 GHz were used to retrieve LWP as described in the next paragraph.

Information on integrated water vapor (IWV) and liquid water path (LWP) was taken from the 14-channel microwave
radiometer (MWR) HATPRO at AWIPEV. Details on the HATPRO retrievals can be found in Nomokonova et al. (2019). The
1-s MWR measurements were averaged to a common 9-s temporal grid similar to the ICON-LEM model output. Since the
120 HATPRO was not measuring between June 21 and June 24 and had also a few data gaps on other days, we took additional
LWP information from a statistical retrieval based on the additional passive 89 GHz channel of the cloud radar. For this LWP
retrieval, we combined 89 GHz brightness temperature measurements with IWV information from GPS. In the case that the
HATPRO LWP is not available but the LWP from the 89 GHz retrieval is, the latter one is used instead, resulting in a combined,
best-estimate data set for LWP. For the analysis of the power spectrum, continuous data are crucial. We thus divided the time
125 series into 6-h intervals and excluded those intervals from the analysis which still suffered from data gaps.

While the cloud radar reflectivity profiles provide information on the vertical occurrence of hydrometeors, more detailed in-
formation on hydrometeor type is provided by the Cloudnet target classification product (Illingworth et al., 2007; Nomokonova
et al., 2019). For this classification, each radar height bin is classified with respect to the occurrence of cloud liquid droplets,
ice, melting ice and drizzle/rain and finally, the profiles of cloud radar reflectivity, Doppler velocity, and of ceilometer atten-
130 uated backscatter are combined with numerical weather prediction data. The resulting classification profiles have the same
temporal (30 s) and vertical (20 m) resolution as the cloud radar measurements.

3 Basic evaluation of clouds

We use the Cloudnet target classification for the initial assessment of the general representation of structure, type and timing
of the modeled versus the observed clouds. The Cloudnet classification also provides an impression of the changing meteoro-
135 logical conditions e.g. frontal passages or occurrence of low-level mixed-phase clouds. The classification of the model output
is based on a threshold of 10^{-8} kg/kg for the hydrometeors and shows a reasonable agreement (Fig. 2) to the Cloudnet classi-
fication described in the previous section. The general situation is mostly captured by the models and also type, structure and
timing are represented well. Nevertheless, some differences especially in the duration of mixed-phase clouds can be spotted
immediately. With regards to resolution, the 2 km resolution already shows a reasonable agreement, even though it has a ten-

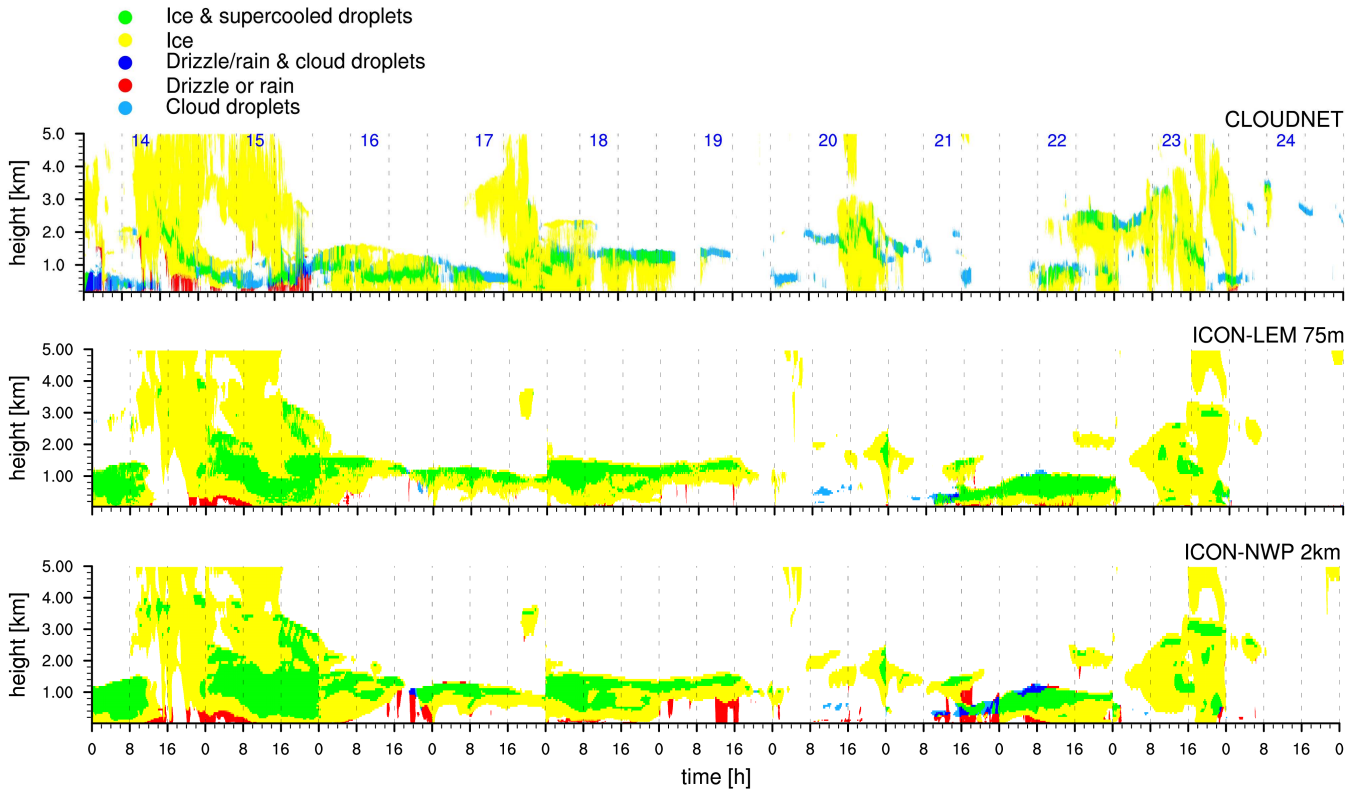


Figure 2. Hydrometeor classification for the whole time series for the observations (Cloudnet classification; top), the ICON-LEM 75 m (middle), and the ICON-NWP 2 km forcing data.

140 dency to generate more precipitation. However, it shows that the large-eddy-simulation benefits from a good representation of
 145 the large-scale atmospheric forcing in the numerical weather prediction data.

The variability of the atmospheric conditions during the 11 days has already been indicated by the Cloudnet classification but can also be seen in the timeseries of IWV and LWP (Fig. 3). For the IWV (top), both resolutions follow nicely the observed general trend. As the IWV is mainly dominated by larger scales, hardly any difference can be seen between the lowest (600 m) and highest (75 m) horizontal resolution. Strong gradients often occur at 0 UTC, which are due to the new model initialization at 0 UTC. The model output between 0 and 6 UTC should be treated with caution as it includes the model spinup but is shown here for completeness. For the LWP (bottom), the models also capture most of the clouds and variability, even though some clouds are missing, which could already be seen in the classification (Fig. 2). For the LWP, the two different ICON-LEM resolutions deviate from each other which is analyzed and shown in more detail in section 5.2.

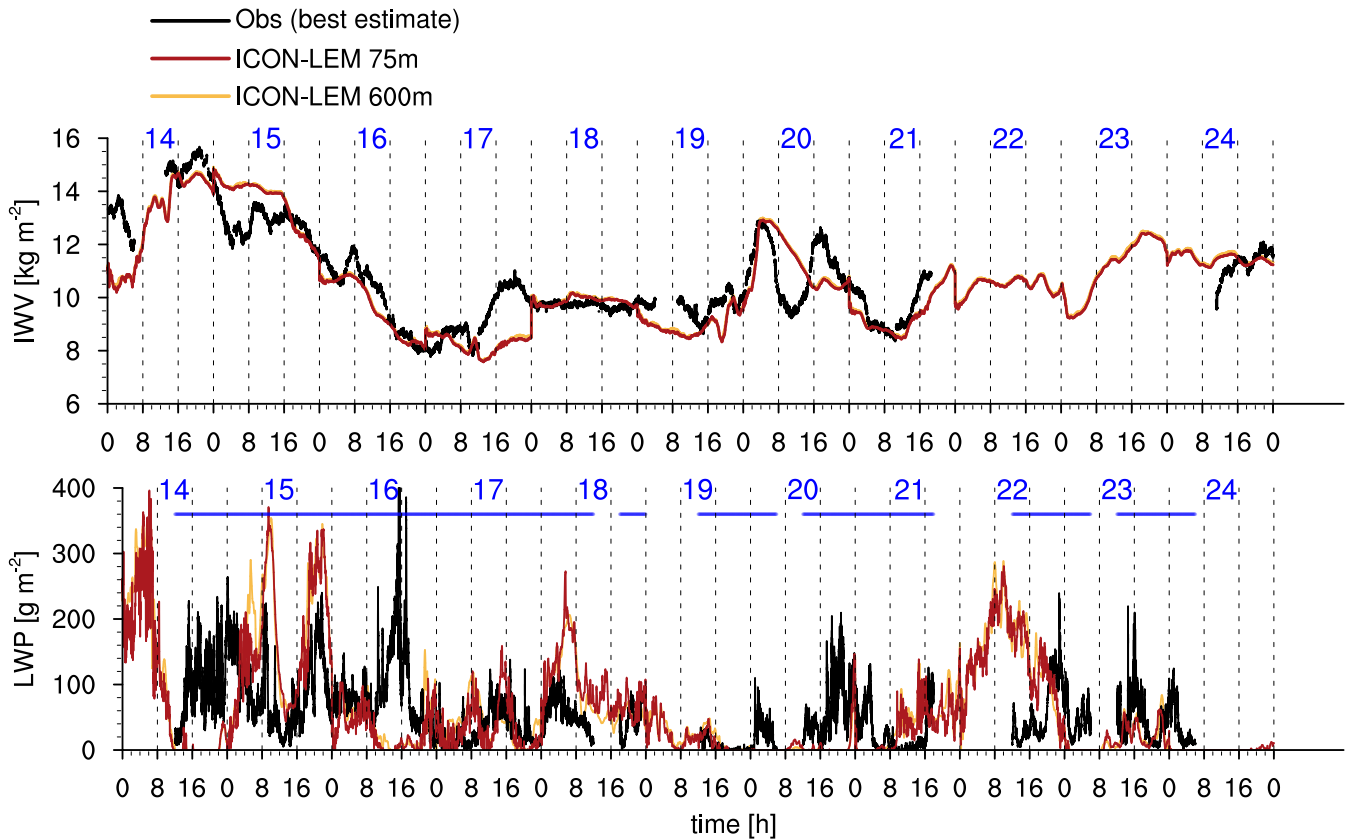


Figure 3. Time series of observed (black) and of ICON-LEM simulated (600 m: yellow, 75 m: red) IWV (top) and LWP (bottom). Blue lines show data availability of the observations.

150 4 Zooming in: Case study 23 June 2017

The previous section showed that the 2 km forcing data already capture the general structure, type and timing of the clouds during the analyzed time period. The very similar classification time series of ICON-LEM and ICON-NWP indicate that the representation in the ICON-LEM is strongly influenced by the forcing data. We will thus investigate the forcing dependency in more detail by focusing on 23 June 2017 which reveals a complicated cloud structure with a very thin mixed-phase cloud and
 155 several liquid layers.

4.1 Forcing dependency

The 23 June 2017 case is a very strong example of the impact of different forcing models on the representation of mixed-phase clouds in the ICON-LEM. Figure 4 shows the hydrometeor classification of this day – again for the observations and the ICON-LEM but also for the 75 m output of the ICON-LEM forced by IFS data. The bottom panels in Fig. 4 show the
 160 forcing data itself. While the ice cloud is represented in all forcing data, it is evaporated immediately and not fully recovered

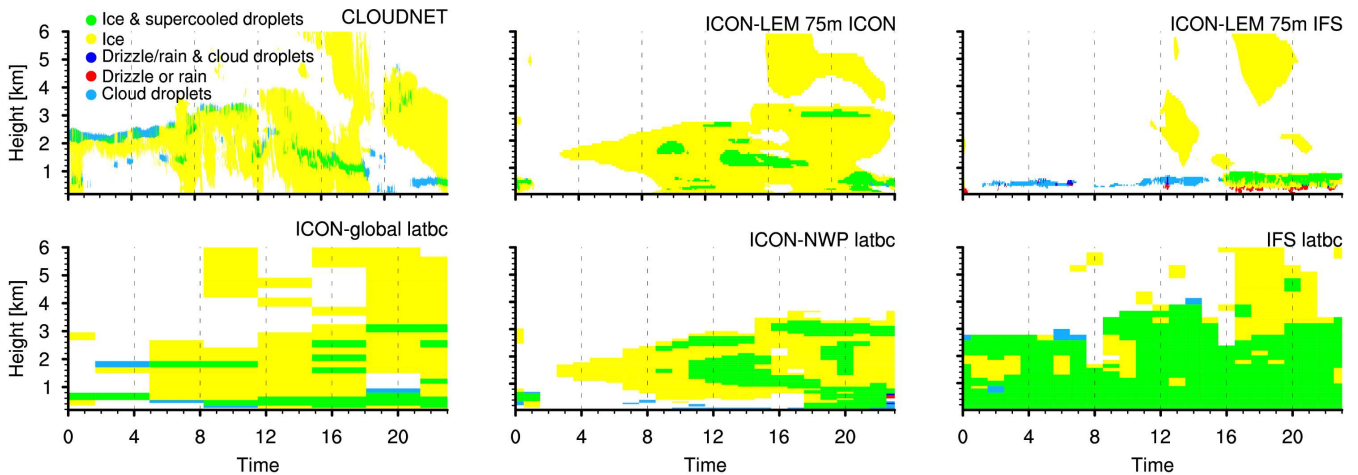


Figure 4. Classification for the case study of 23 June 2017 showing the observations (top, left) the ICON-LEM results at 75 m resolution with forcing from the ICON family (top middle) and forcing from the IFS (top right). The respective forcing data for the lateral boundary conditions (latbc) from the operational global ICON (ICON-global; bottom left), the ICON at 2 km resolution (ICON-NWP; bottom middle) and from the IFS (bottom right) are also shown.

in the ICON-LEM simulation forced with the IFS data. The reason for the sudden evaporation is probably a different set of parameterizations and the relation between subgrid-scale (ice) clouds and the mean state in the models. The transition to a different state representation in the ICON model leads to a mismatch. The ICON-LEM with a 75 m resolution and forced by the ICON model chain captures the cloud situation with low- and mid-level mixed-phase clouds and higher ice cloud in the afternoon much better than the one forced with the IFS. The mixed-phase clouds around 2 km height in the beginning of the day are not captured by ICON-LEM which might still be connected to the spin-up time of the model. This example shows the importance of applying consistent forcing data, which is possible with the new ICON suite that can simulate at scales ranging from climate to large-eddy-resolving.

4.2 Vertical structure of the clouds

While the general structure is captured in the ICON-LEM simulation with the ICON forcing, we are also interested in the composition of the clouds and the dominating microphysical properties and processes. On the one hand, cloud properties which have been retrieved from observations could be directly compared to the model results. However, retrieval algorithms applied to measurements may induce large uncertainties in this comparison. On the other hand, the modeled mixed-phase cloud properties can be evaluated by comparing observed cloud radar reflectivities with forward simulated reflectivities based on the ICON-LEM model output. Figure 5 shows the observed reflectivities as well as the ones from the ICON-LEM which were forward simulated with the Passive and Active Microwave TRAnsfer model (PAMTRA; (Maahn et al., 2015)). Radar reflectivity depend on both hydrometeor concentration and size. We consistently find that the simulated reflectivities are lower than the observed ones. This underestimation might indicate that the ICON-LEM clouds consist of too small particles. One

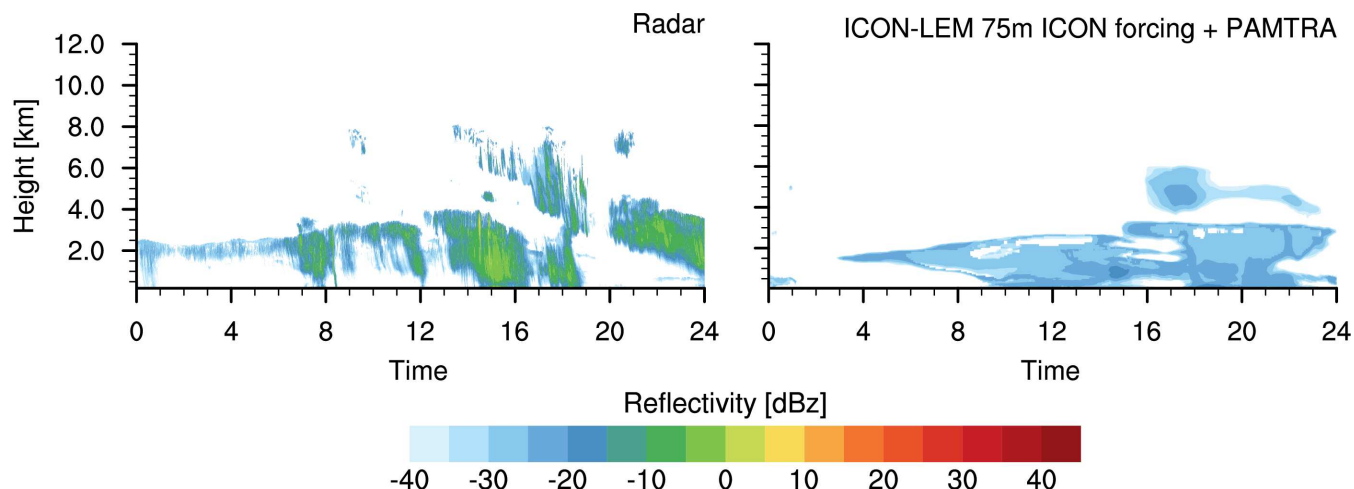


Figure 5. Time series of observed (left) and simulated cloud radar reflectivity based on the ICON-LEM with 75 m resolution (right) for the case study of 23 June 2017.

possible explanation could be the limitation of the applied CCN and IN parameterization. Another issue could be in the
 180 description of growing processes for the ice clouds.

5 Statistical evaluation

While case studies allow us to investigate certain situations in detail, they might not be representative for the general model behaviour. In this section, we use all 11 days to tackle the question of how well the microphysical composition of the clouds is represented in the simulations and how much information can be added by higher horizontal resolutions.

185 5.1 Reflectivity distribution

As the ice cloud on 23 June 2017 is very thin and challenging for the model (as seen in the previous section), the underestimation of the radar reflectivity might not be representative for the general model behaviour. We thus compare the observed and simulated reflectivities for all 11 days in a 2D histogram (Fig. 6). The frequencies are based on the total number of possible data points (e.g. 9600 for the model output). With this approach, the distributions provide information about the total frequency
 190 at all heights simultaneously. Interestingly, in the model, radar reflectivities are basically confined to values between -32 and -20 dBZ with two distinct peaks around -29 dBZ and -23 dBZ. Up to 1.5 km height, observed radar reflectivities range between -36 to -24 dBZ. Such a higher occurrence of radar reflectivities can also be seen in the model. The histogram confirms the results of the case study that the simulated reflectivities tend to be too low compared to the observed ones. This becomes even more clear for the clouds around 3 km height, where the observed frequencies shift towards higher values, while the simulated
 195 ones stay close at -30 dBZ. However, the observed and the simulated reflectivities cover in principal the same range indicating

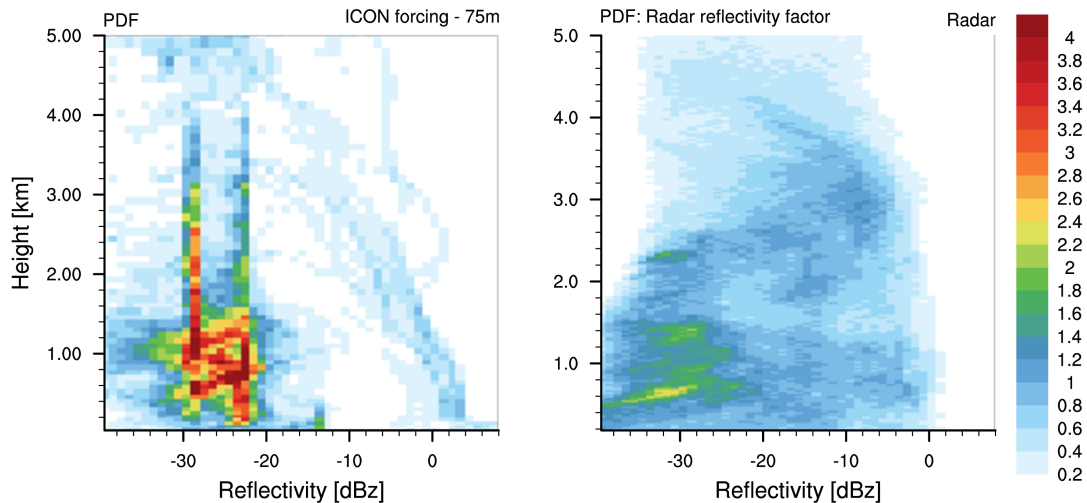


Figure 6. 2D histogram for simulated (left) and observed (right) radar reflectivities for all 11 days (14-24 June 2017). The PDF (%) of each height is based on the maximal possible number of datapoints (normalized).

the potential to reach a better representation by refined microphysical parameterizations. The too high occurrence of simulated low radar reflectivities and the two distinct peaks go along with very small and persistent ice water contents (not shown) and might be due to overestimated ice nucleation particles (IN) and cloud condensation particles (CCN) number concentrations. In order to better explain the differences between simulated and observed radar reflectivities more detailed sensitivity studies are needed disentangling the effects of CCN, IN, and microphysical processes. This will be part of future research with upcoming long-term measurements of IN and CCN.

5.2 Resolution dependency

When looking at the general representation of the cloud structure as given by the hydrometeor classification (Fig. 2), the difference between different resolutions of ICON was rather small. In this section, a more detailed analysis of the impact of the different resolution will be presented. The analysis is performed on the meteorogram output, which has an output frequency of 9 s and approaches the temporal scale of the observations. Being able to compare observations and model output at similar scales, is one of the key argument for high-resolution simulations. Still, the questions remain on which scales variability is resolved by the model and which resolution is needed to resolve the main part of the observed variability. Figure 7 qualitatively shows how the structure of resolved features gets finer and more detailed with increasing resolution, i.e. 600 m, 300 m, 150 m, and 75 m, from the outer to the inner circles. To quantify this first impression, we calculated the power spectrum of the integrated quantities (LWP, IWV and IWP). Due to data availability, we divided the days into four parts each 6 hour long and picked the sequences with full data availability (see section 2.2 and Fig. 3 for details). For each 6 hour time series, we calculated the power density spectrum $P(f_i)$ for the frequencies $F = [\Delta f, \dots, \frac{1}{2\Delta}]$, where Δ is the smallest time interval of the dataset. As the forcing data is produced at a different time frequency, we divided each power density spectrum by the bin width Δf to be

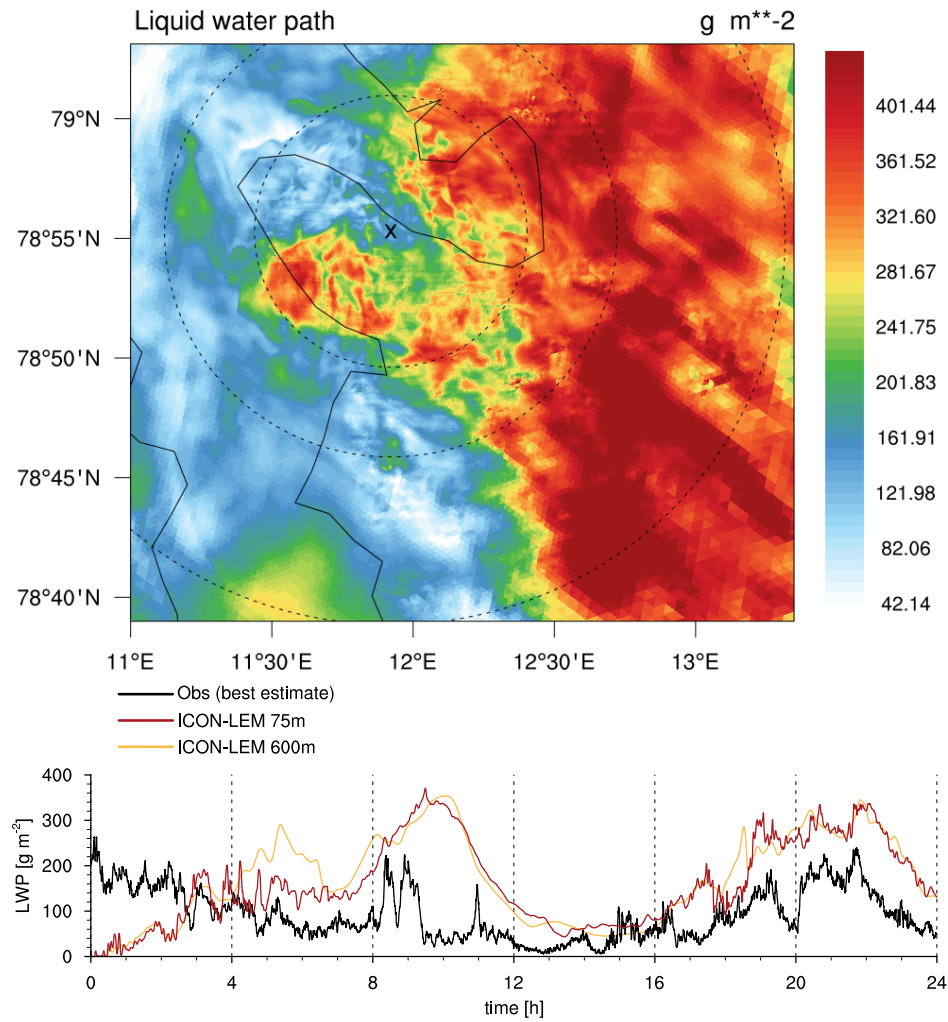


Figure 7. Snapshot of the LWP at 15 June 2017 6:30 pm showing an overlay of all four different resolutions (top), where the dashed lines are indicating the size of the different domains, the solid line the coast, and the x the location of Ny-Ålesund. And a LWP time series for the the same day showing the best estimate of the observations and the coarsest (600 m) as well as finest (75 m) ICON-LEM resolution.

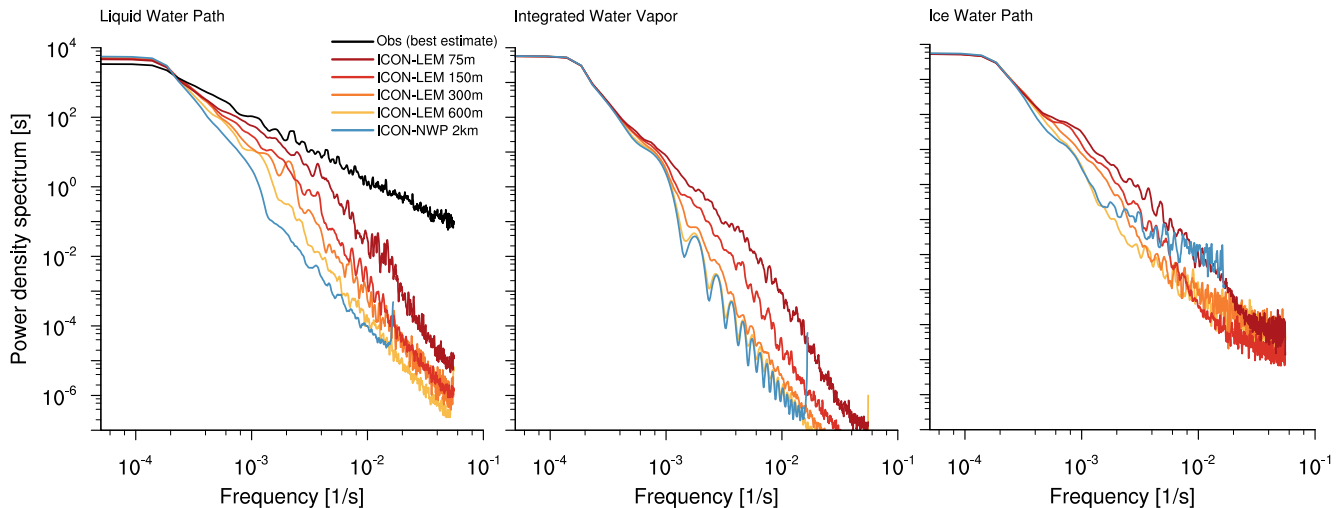


Figure 8. Power density spectrum for LWP (left), IWV (middle) and IWP (right) for the forcing ICON-NWP (blue) and the ICON-LEM for the four different resolutions ranging from 600 m (yellow) to 75 m (dark red). For LWP also the observations are shown (black). The spectrum is averaged over several 6 hour time slots excluding 0-6 hour every morning due to spin up and time slots without available observations (see Fig. 3).

215 independent of the bin width. As the total amount of variance differs between the simulations and the observations, and we are interested in the scaling behavior, the power density spectrum has been normalized by the total variance

$$p(f_i) = \frac{P(f_i)}{\Delta f} \frac{1}{\sum_{f_j \in F} P(f_j)} \quad (1)$$

Figure 8 shows the normalized power density spectrum for the observations, the four different resolutions of the ICON-LEM and the 2 km ICON-NWP. Since continuous highly resolved (i.e. here 9 s) IWV and IWP observations are not available, only the retrieved LWP is shown in the analysis. While especially for the forcing data the resolved variability is dominated by the large scales, we see an increase of variability at smaller scales with the four ICON-LEM resolutions. Especially for the 75 m resolution, the model approaches the variability of the observations. While, of course, the observations also contain a certain amount of noise – which might dominate the small scale variability – it could be an interesting experiment in the future to test even higher model resolutions. For now we see a clear improvement in the representation of the small scale variability by increasing the resolution from 600 m to 75 m.

For IWV and IWP (see Fig. 8) the behavior is very similar. The highest resolution resolves more energy at smaller scales than the coarser resolutions. While the IWV spectrum decays very quickly with smaller scales, the IWP spectrum decays later, more similar to the LWP. This shows that the IWV is mainly large-scale driven while for IWP and LWP smaller scales and fluctuations play a more important role, even though they are still partly unresolved in the model as the comparison with the observations for the LWP clearly shows.

5.3 Testing the representativity

The complex terrain around Ny-Ålesund is also a further challenge for point-to-point comparisons between the model and the observations. A slight mismatch in the location of the compared model column might already lead to a completely different environment compared to the observational site. For this reason, we are interested in the question of how strongly neighbouring columns vary, and if a point-to-point comparison is meaningful at all. This question is a subaspect of the longstanding question of how representative measurements at a supersite like Ny-Ålesund are for Arctic regions in general. The model allows us to slowly approach these questions. To show the potential, we take the coarse 2 km ICON simulations and select four different small sub-regions with different environments (Fig. 9, left): the coastal site Ny-Ålesund, sea-ice, open water and mixed conditions (where both sea ice and open water occur). For each of these places, we pick 10 neighbouring cells and compare the PDF of LWP of the 9 outer ones with the original cell in the center to estimate the local variability. The PDFs are compared based on their mean value and the Hellinger distance, which can be used to compare also discrete distributions:

$$H(C, N) = \frac{1}{\sqrt{2}} \|\sqrt{C} - \sqrt{N}\|_2 = \frac{1}{\sqrt{2}} \sqrt{\sum_{i=1}^k (\sqrt{c_i} - \sqrt{n_i})^2},$$

with $0 \leq H(C, N) \leq 1$, and C being the PDF of the original cell and N of a single neighbouring cell ($N \in \{N_1, \dots, N_9\}$). For identical distributions, H equals zero. The maximum distance $H = 1$ is achieved for completely disjunct PDFs, which do not overlap.

We see, that - as could be expected - the differences of the PDFs are smallest for open water and sea ice conditions. Under mixed conditions close to the fjord, we already see larger differences among the 9 grid points as indicated by a slightly larger Hellinger distance and larger variations in the mean value of LWP. Clearly, we find the largest Hellinger distance for Ny-Ålesund as well as the largest differences in the LWP mean values. For a horizontal resolution of approximately 2 km this is certainly expected as the neighbouring grid cells might be characterized by very different surfaces - e.g. coast, mountains, fjord, and glaciers. The larger Hellinger distance and the increased variability of the mean LWP around Ny-Ålesund compared to the other points shows that the local features are captured by the model. Certainly the point-to-point comparison has to be done carefully for Ny-Ålesund, but the fact that the local features can be seen by the model is promising for a reasonable representation of the column output. In future, measurements from a scanning MWR can be used to also describe the spatial variability of LWP from the observations and set this one then directly into context to the model LWP fields. At the moment we can only evaluate the model output at Ny-Ålesund and the small differences over water or sea ice might also be due to a too simplistic representation within the model. Upcoming campaigns (e.g. MOSAiC) will enable us to also evaluate the model under varying conditions, as over sea ice. Then the model can be evaluated and tested at observational anchor sites but will provide information on larger domains - e.g. covering the whole Arctic - enabling the comparison of Ny-Ålesund to a larger region.

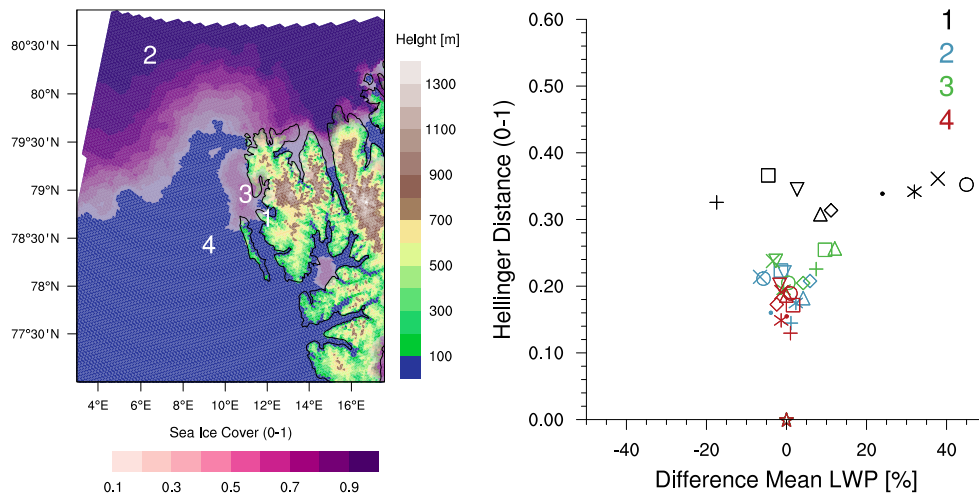


Figure 9. Left: Location of the four 10-grid point subregions used for the representativity analysis: land (1), sea ice (2), mixed conditions (sea ice and open water) (3), open water (4). Right: Hellinger distance and differences in mean LWP of the LWP PDFs of the surrounding grid points (different symbols) compared to the central point (star symbol) for the four subregions. Values have been calculated for each day and then averaged over all 11 days.

6 Conclusions

Low-level mixed-phase clouds, which are very common in the Arctic (Shupe et al., 2008), have a substantial impact on the redistribution of radiative energy in the Arctic (e.g. Ebell et al., 2019; Miller et al., 2015) and are driven by very complex processes (Morrison et al., 2012). Thus, their representation is a challenge for today's climate models (Pithan et al., 2014). To improve the respective parameterizations and our process-level understanding, we need tools like a combination of detailed as well as long-term observations and high-resolution models. In this study, we presented the first simulations with the new
 265
 270
 275

ICON-LEM under Arctic conditions and the complex terrain of Ny-Ålesund. We demonstrated its capability to capture the general structure, type and timing of the observed mixed-phase clouds. By analyzing 11 days during the ACLOUD campaign, we showed the potential for more detailed studies focusing on the composition of mixed-phase clouds and the dominating microphysical processes. To understand microphysical processes, it is important to bring the simulations and the observations on a similar scale, which can only be done with high resolutions. While the overall structure of the observed clouds is already captured in general by the large-scale forcing, we showed large differences, especially for the variability of the LWP, between the different resolutions. While certainly also a 75 m resolution is still too coarse for convergence and higher resolutions might still add more information, we could already see a distinct information gain from the lower (2 km, 600 m, 300 m, 150 m) to the highest ICON resolution (75 m).

For the high-resolution model, we chose a rather small domain, which increases the dependency on the large-scale forcing and by that the induced uncertainty. Based on a case study, we demonstrated the effect of using two different forcing data sets as well as the benefit of having a consistent forcing with a similar model. This consistent forcing can be achieved with the new

ICON model suite, which allows simulations on scales reaching from the global and climate scales to Large-Eddy-resolving
280 scales. Even though the parameterizations still have to be exchanged or switched off, the definition of the atmospheric state
and the dynamics stay the same, which is a great advantage and reduces the uncertainty in the high-resolution simulations as
well as the necessary spin-up time.

We found a persistent underestimation of radar reflectivity in the simulations, which hints at too small particles and could
be due to the applied CCN and IN background forcing. Especially in the clean Arctic regime, the sensitivity on CCN and IN
285 might be higher than in the mid-latitudes and should be investigated in more detail also in the ICON-LEM setup.

One long-standing question is the representativity of point measurements in general and especially at complex locations
like Ny-Ålesund. We presented a first attempt to show the potential of high-resolution modeling to tackle these questions
by offering a four-dimensional context to the point measurements. In future, it is necessary to evaluate the model also under
different conditions like sea-ice in the central Arctic. Upcoming campaigns like MOSAiC will offer the necessary observational
290 data sets and open up new possibilities for the synthesis of high-resolution modeling and observations in the Arctic.

The presented combination of long-term as well as state-of-the-art observations and the novel ICON model suite - including
the ICON-LEM - can lead to an improved process understanding and therefore to a better representation also in the large-scale
models, which will allow us to investigate feedback and climate mechanisms related to Arctic Amplification in more detail.

Data availability. ICON-LEM model data are available at the tape archive of the German Climate Computing Center (DKRZ;
295 <https://www.dkrz.de/up/systems/hpss/hpss>); one needs to register at DKRZ to get a user account. We will also make the data available via
Swift (<https://www.dkrz.de/up/systems/swift>) on request. The Cloudnet data are available at the Cloudnet website (<http://devcloudnet.fmi.fi/>,
Cloudnet, 2018). The IWV data of the MWR are available at PANGAEA (<https://doi.pangaea.de/10.1594/PANGAEA.902142>).

Author contributions. VS performed the model simulations and the respective analysis of the model output. KE processed the observational
data and supported the analysis. Both prepared the manuscript.

300 *Competing interests.* The authors declare that they have no conflict of interest.

Acknowledgements. We gratefully acknowledge the funding by the Deutsche Forschungsgemeinschaft (DFG, German Research Foundation)
– project number 268020496 – TRR 172, within the Transregional Collaborative Research Center “Arctic Amplification: Climate Relevant
Atmospheric and SurfaCe Processes, and Feedback Mechanisms (AC)³, and the computing time granted on the supercomputer MISTRAL at
Deutsches Klimarechenzentrum GmbH (DKRZ) through its Scientific Steering Committee (WLA). We acknowledge the ACTRIS-2 project
305 (European Commission contract H2020-INFRAIA, grant no. 654109) for providing the target classification, which was produced by the
Finnish Meteorological Institute using measurements from Ny-Ålesund. We thank Mario Mech for performing the forward simulations with

PAMTRA for the model output and Christoph Ritter and Marion Maturilli of the Alfred Wegener Institute, Helmholtz Centre for Polar and Marine Research, Potsdam, for providing MWR and ceilometer data used in the Cloudnet algorithms, respectively. We also thank AWIPEV for hosting the cloud radar of University of Cologne and the AWIPEV team for helping us in the instrument operation.

310 **References**

- Dipankar, A., Stevens, B., Heinze, R., Moseley, C., Zängl, G., Giorgetta, M., and Brdar, S.: Large eddy simulation using the general circulation model ICON, *Journal of Advances in Modeling Earth Systems*, 7, 963–986, <https://doi.org/10.1002/2015MS000431>, 2015.
- Ebell, K., Nomokonova, T., Maturilli, M., and Ritter, C.: Radiative effect of clouds at Ny-Ålesund, Svalbard, as inferred from ground-based remote sensing observations, *Journal of Applied Meteorology and Climatology*, <https://doi.org/10.1175/JAMC-D-19-0080.1>, 2019.
- 315 Gierens, R., Kneifel, S., Shupe, M. D., Ebell, K., Maturilli, M., and Löhnert, U.: Low-level mixed-phase clouds in a complex Arctic environment, *Atmospheric Chemistry and Physics Discussions*, 2019, 1–37, <https://doi.org/10.5194/acp-2019-610>, <https://www.atmos-chem-phys-discuss.net/acp-2019-610/>, 2019.
- Goosse, H., Kay, J. E., Armour, K. C., Bodas-Salcedo, A., Chepfer, H., Docquier, D., Jonko, A., Kushner, P. J., Lecomte, O., Massonnet, F., Park, H.-S., Pithan, F., Svensson, G., and Vancoppenolle, M.: Quantifying climate feedbacks in polar regions, *Nature Commun.*, 9, <https://doi.org/10.1038/s41467-018-04173-0>, 2018.
- 320 Hande, L. B., Engler, C., Hoose, C., and Tegen, I.: Parameterizing cloud condensation nuclei concentrations during HOPE, *Atmospheric Chemistry and Physics*, 16, 12 059–12 079, <https://doi.org/10.5194/acp-16-12059-2016>, <https://www.atmos-chem-phys.net/16/12059/2016/>, 2016.
- Heinze, R., Dipankar, A., Henken, C. C., Moseley, C., Sourdeval, O., Trömel, S., Xie, X., Adamidis, P., Ament, F., Baars, H., Barthlott, C., Behrendt, A., Blahak, U., Bley, S., Brdar, S., Brueck, M., Crewell, S., Deneke, H., Di Girolamo, P., Evaristo, R., Fischer, J., Frank, C., Friederichs, P., Göcke, T., Gorges, K., Hande, L., Hanke, M., Hansen, A., Hege, H.-C., Hoose, C., Jahns, T., Kalthoff, N., Klocke, D., Kneifel, S., Knippertz, P., Kuhn, A., van Laar, T., Macke, A., Maurer, V., Mayer, B., Meyer, C. I., Muppa, S. K., Neggers, R. A. J., Orlandi, E., Pantillon, F., Pospichal, B., Röber, N., Scheck, L., Seifert, A., Seifert, P., Senf, F., Siligam, P., Simmer, C., Steinke, S., Stevens, B., Wapler, K., Weniger, M., Wulfmeyer, V., Zängl, G., Zhang, D., and Quaas, J.: Large-eddy simulations over Germany using
- 330 ICON: a comprehensive evaluation, *Quarterly Journal of the Royal Meteorological Society*, 143, 69–100, <https://doi.org/10.1002/qj.2947>, <https://rmets.onlinelibrary.wiley.com/doi/abs/10.1002/qj.2947>, 2017.
- Illingworth, A. J., Hogan, R. J., O'Connor, E. J., Bounoil, D., Brooks, M. E., Delanoë, J., Donovan, P., Eastment, J. D., Gaussiat, N., Goddard, J. W. F., Haeffelin, M., Klein, H., Baltink, H. K., Krasnov, O. A., Pelon, J., Piriou, J.-M., Protat, A., Russchenberg, H. W. J., Seifert, A., Tompkins, A. M., van Zadelhoff, G.-J., Vinit, F., Willén, U., Wilson, D. R., and Wrench, C. L.: CLOUDNET Continuous evaluation of
- 335 cloud profiles in seven operational models using ground-based observations, *Bull. Amer. Meteor. Soc.*, 88, 883–898, 2007.
- Klein, S. A., McCoy, R. B., Morrison, H., Ackerman, A. S., Avramov, A., Boer, G. d., Chen, M., Cole, J. N. S., Del Genio, A. D., Falk, M., Foster, M. J., Fridlind, A., Golaz, J.-C., Hashino, T., Harrington, J. Y., Hoose, C., Khairoutdinov, M. F., Larson, V. E., Liu, X., Luo, Y., McFarquhar, G. M., Menon, S., Neggers, R. A. J., Park, S., Poellot, M. R., Schmidt, J. M., Sednev, I., Shipway, B. J., Shupe, M. D., Spangenberg, D. A., Sud, Y. C., Turner, D. D., Veron, D. E., Salzen, K. v., Walker, G. K., Wang, Z., Wolf, A. B., Xie, S., Xu, K.-M., Yang,
- 340 F., and Zhang, G.: Intercomparison of model simulations of mixed-phase clouds observed during the ARM Mixed-Phase Arctic Cloud Experiment. I: single-layer cloud, *Quarterly Journal of the Royal Meteorological Society*, 135, 979–1002, <https://doi.org/10.1002/qj.416>, 2009.
- Küchler, N., Kneifel, S., Löhnert, U., Kollias, P., Czekala, H., and Rose, T.: A W-Band Radar-Radiometer System for Accurate and Continuous Monitoring of Clouds and Precipitation, *J. Atmos. Oceanic Technol.*, 34, 2375–2392, <https://doi.org/10.1175/JTECH-D-17-0019.1>,
- 345 2017.

- Loewe, K., Ekman, A. M., Paukert, M., Sedlar, J., Tjernström, M., and Hoose, C.: Modelling micro- and macrophysical contributors to the dissipation of an Arctic mixed-phase cloud during the Arctic Summer Cloud Ocean Study (ASCOS), *Atmos. Chem. Phys.*, 17, 6693–6704, <https://doi.org/10.5194/acp-17-6693-2017>, 2017.
- Maahn, M., Löhnert, U., Kollias, P., Jackson, R. C., and McFarquhar, G. M.: Developing and Evaluating Ice Cloud Parameterizations for Forward Modeling of Radar Moments Using in situ Aircraft Observations, *J. Atmos. Oceanic Technol.*, 32, 880–903, <https://doi.org/10.1175/JTECH-D-14-00112.1>, 2015.
- Marke, T., Crewell, S., Schemann, V., Schween, J. H., and Tuononen, M.: Long-Term Observations and High-Resolution Modeling of Midlatitude Nocturnal Boundary Layer Processes Connected to Low-Level Jets, *Journal of Applied Meteorology and Climatology*, 57, 1155–1170, <https://doi.org/10.1175/JAMC-D-17-0341.1>, 2018.
- 355 Maturilli, M. and Kayser, M.: Arctic warming, moisture increase and circulation changes observed in the Ny-Ålesund homogenized radiosonde record, *Theor. Appl. Climatol.*, 130, 1–17, <https://doi.org/10.1007/s00704-016-1864-0>, 2017.
- Maturilli, M., Herber, A., and König-Langlo, G.: Climatology and time series of surface meteorology in Ny-Ålesund, Svalbard, *Earth System Science Data*, 5, 155–163, <https://doi.org/10.5194/essd-5-155-2013>, <https://www.earth-syst-sci-data.net/5/155/2013/>, 2013.
- Maturilli, M., Herber, A., and König-Langlo, G.: Surface radiation climatology for Ny-Ålesund, Svalbard (78.9° N), *Theor. Appl. Climatol.*, 360 120, 331–339, <https://doi.org/10.1007/s00704-014-1173-4>, 2015.
- Miller, N. B., Shupe, M. D., Cox, C. J., Walden, V. P., Turner, D. D., and Steffen, K.: Cloud Radiative Forcing at Summit, Greenland, *Journal of Climate*, 28, 6267–6280, <https://doi.org/10.1175/JCLI-D-15-0076.1>, 2015.
- Morrison, H., de Boer, G., Feingold, G., Harrington, J., Shupe, M. D., and Sulia, K.: Resilience of persistent Arctic mixed-phase clouds, *Nature Geoscience*, 5, 11–17, 2012.
- 365 Neggers, R. A. J., Chylik, J., Egerer, U., Griesche, H., Schemann, V., Seifert, P., Siebert, H., and Macke, A.: Local and remote controls on Arctic mixed-layer evolution, *Journal of Advances in Modeling Earth Systems*, 0, <https://doi.org/10.1029/2019MS001671>, 2019.
- Nomokonova, T., Ebell, K., Löhnert, U., Maturilli, M., Ritter, C., and O’Connor, E.: Statistics on clouds and their relation to thermodynamic conditions at Ny-Ålesund using ground-based sensor synergy, *Atmos. Chem. Phys.*, 19, 1–22, <https://doi.org/10.5194/acp-19-1-2019>, 2019.
- 370 Ovchinnikov, M., Ackerman, A. S., Avramov, A., Cheng, A., Fan, J., Fridlind, A. M., Ghan, S., Harrington, J., Hoose, C., Korolev, A., McFarquhar, G. M., Morrison, H., Paukert, M., Savre, J., Shipway, B. J., Shupe, M. D., Solomon, A., and Sulia, K.: Intercomparison of large-eddy simulations of Arctic mixed-phase clouds: Importance of ice size distribution assumptions, *Journal of Advances in Modeling Earth Systems*, 6, 223–248, <https://doi.org/10.1002/2013MS000282>, 2014.
- Pithan, F., Medeiros, B., and Mauritsen, T.: Mixed-phase clouds cause climate model biases in Arctic wintertime temperature inversions, 375 *Climate Dynamics*, 43, 289–303, <https://doi.org/10.1007/s00382-013-1964-9>, 2014.
- Screen, J. A., Deser, C., Smith, D. M., Zhang, X., Blackport, R., Kushner, P. J., Oudar, T., McCusker, K. E., and Sun, L.: Consistency and discrepancy in the atmospheric response to Arctic sea-ice loss across climate models, *Nature Geosc.*, 11, 155–163, <https://doi.org/10.1038/s41561-018-0059-y>, 2018.
- Seifert, A. and Beheng, K. D.: A two-moment cloud microphysics parameterization for mixed-phase clouds. Part 1: Model description, 380 *Meteorology and Atmospheric Physics*, 92, 45–66, <https://doi.org/10.1007/s00703-005-0112-4>, 2006.
- Serreze, M. C. and Barry, R. G.: Processes and impacts of Arctic amplification: A research synthesis, *Global Planet. Change*, 77, 85–96, <https://doi.org/10.1016/j.gloplacha.2011.03.004>, 2011.

- Shupe, M. D., Matrosov, S. Y., and Uttal, T.: Arctic Mixed-Phase Cloud Properties Derived from Surface-Based Sensors at SHEBA, *Journal of the Atmospheric Sciences*, 63, 697–711, <https://doi.org/10.1175/JAS3659.1>, 2006.
- 385 Shupe, M. D., Daniel, J. S., DeBoer, G., Eloranta, E. W., Kollias, P., Long, C. N., Luke, E. P., Turner, D. D., and Verlinde, J.: A focus on mixed-phase clouds, *Bull. Amer. Meteor. Soc.*, 89, 1549–1562, 2008.
- Tjernström, M., Shupe, M. D., Brooks, I. M., Achtert, P., Prytherch, J., and Sedlar, J.: Arctic Summer Airmass Transformation, Surface Inversions, and the Surface Energy Budget, *Journal of Climate*, 32, 769–789, <https://doi.org/10.1175/JCLI-D-18-0216.1>, 2019.
- Wendisch, M., Brückner, M., Burrows, J. P., Crewell, S., Dethloff, K., Ebell, K., Lüpkes, C., Macke, A., Notholt, J., Quaas, J., Rinke, A.,
390 and Tegen, I.: Understanding causes and effects of rapid warming in the Arctic, *Eos*, 98, 22–26, <https://doi.org/10.1029/2017EO064803>, 2017.
- Wendisch, M., Macke, A., Ehrlich, A., Lüpkes, C., Mech, M., Chechin, D., Dethloff, K., Velasco, C. B., Bozem, H., Brückner, M., Clemen, H.-C., Crewell, S., Donth, T., Dupuy, R., Ebell, K., Egerer, U., Engelmann, R., Engler, C., Eppers, O., Gehrmann, M., Gong, X., Gottschalk, M., Gourbeyre, C., Griesche, H., Hartmann, J., Hartmann, M., Heinold, B., Herber, A., Herrmann, H., Heygster, G., Hoor, P.,
395 Jafariserajehlou, S., Jäkel, E., Järvinen, E., Jourdan, O., Kästner, U., Kecorius, S., Knudsen, E. M., Köllner, F., Kretzschmar, J., Lelli, L., Leroy, D., Maturilli, M., Mei, L., Mertes, S., Mioche, G., Neuber, R., Nicolaus, M., Nomokonova, T., Notholt, J., Palm, M., van Pinxteren, M., Quaas, J., Richter, P., Ruiz-Donoso, E., Schäfer, M., Schmieder, K., Schnaiter, M., Schneider, J., Schwarzenböck, A., Seifert, P., Shupe, M. D., Siebert, H., Spreen, G., Stapf, J., Stratmann, F., Vogl, T., Welti, A., Wex, H., Wiedensohler, A., Zanatta, M., and Zeppenfeld, S.: The Arctic Cloud Puzzle: Using ALOUD/PASCAL Multiplatform Observations to Unravel the Role of Clouds and Aerosol Particles
400 in Arctic Amplification, *Bulletin of the American Meteorological Society*, 100, 841–871, <https://doi.org/10.1175/BAMS-D-18-0072.1>, 2019.
- Zängl, G., Reinert, D., Rípodas, P., and Baldauf, M.: The ICON (ICOsahedral Non-hydrostatic) modelling framework of DWD and MPI-M: Description of the non-hydrostatic dynamical core, *Quarterly Journal of the Royal Meteorological Society*, 141, 563–579, <https://doi.org/10.1002/qj.2378>, 2015.